

# The Single Photon Signature of a Light Long-lived Neutralino at Remote Detectors at the LHC

---

Herbi K. Dreiner,<sup>a</sup> Julian Günther,<sup>a</sup> Dominik Köhler,<sup>a</sup> Apoorva Shah<sup>a</sup>

<sup>a</sup>*Bethe Center for Theoretical Physics & Physikalisches Institut der Universität Bonn,  
Nußallee 12, 53115 Bonn, Germany*

*E-mail:* [dreiner@uni-bonn.de](mailto:dreiner@uni-bonn.de), [jyahguen@uni-bonn.de](mailto:jyahguen@uni-bonn.de),  
[dkoehler@uni-bonn.de](mailto:dkoehler@uni-bonn.de), [ashah@uni-bonn.de](mailto:ashah@uni-bonn.de)

**ABSTRACT:** We investigate the phenomenology of light long-lived neutralinos in R-parity violating supersymmetric models, focusing on the proposed remote detectors ANUBIS, CODEX-b, FACET, FASER, FASER2, MAPP, MAPP2, and MATHUSLA at the LHC. We assume the production of the neutralinos at the ATLAS or CMS interaction points via rare scalar meson decays induced by R-parity violating couplings. We study six supersymmetric R-parity violating benchmark scenarios in which the dominant neutralino decay is  $\tilde{\chi}_1^0 \rightarrow \gamma + \nu$ . For each scenario, we determine the projected search sensitivity at the above listed detectors. Extending previous work focused primarily on FASER and FASER2, we improve the simulation by taking into account the extended flight path of the parent meson. We find that ANUBIS provides the best sensitivity to our benchmark scenarios and FASER the least among the considered experiments, while of course FASER has already taken data.

---

## Contents

<b>1</b>	<b>Introduction</b>	<b>1</b>
<b>2</b>	<b>Theoretical Framework</b>	<b>3</b>
2.1	The RPV-MSSM	3
2.2	A Long-lived Light Neutralino	4
<b>3</b>	<b>Simulation Procedure</b>	<b>6</b>
<b>4</b>	<b>Results</b>	<b>8</b>
4.1	Benchmark 1	8
4.2	Benchmark 2	13
4.3	Benchmark 3	14
4.4	Benchmark 4	16
4.5	Benchmark 5	17
4.6	Benchmark 6	17
<b>5</b>	<b>Conclusions</b>	<b>18</b>

---

## 1 Introduction

Supersymmetry (SUSY) is a theoretically well-motivated extension of the Standard Model of particle physics (SM) [1–3]. In its minimal form, the so-called Minimal Supersymmetric Standard Model (MSSM) provides a good framework to address many of the open questions of the SM, such as the neutrino masses, the baryon asymmetry and the dark matter in the Universe. For reviews, see for example Refs. [4–8]. As a promising solution to the hierarchy problem [9], supersymmetry could very well manifest itself at energies within reach of current experiments. Efforts searching for physics beyond the SM are underway, spanning a wide range of experimental and observational approaches. These include collider experiments [10] with near or far detectors [11], beam-dump studies [12, 13], nuclear and electron recoil measurements [14], as well as astrophysical observations [15–17].

The ATLAS [18, 19] and CMS [20, 21] collaborations at the LHC have been devoting a large effort in the search for SUSY. See for example Refs. [22, 23]. See also the overview of supersymmetry searches compiled by the Particle Data Group [24]. Although no definitive discovery of such particles has yet been achieved, stringent lower bounds on their masses have been established. For example, squark and

gluino masses are constrained to be higher than  $\mathcal{O}(5 \text{ TeV})$ , depending on the precise supersymmetric model [25, 26].

While most collider searches have focused on R-parity conserving (RPC) SUSY, which typically involves missing transverse momentum signatures, models with R-parity violation (RPV) are equally well-motivated [27–30]. In addition, light neutrinos can arise naturally in RPV models without introducing a new see-saw energy scale [29, 31–33]. Note, in RPV scenarios, any superpartner can in principle be the lightest supersymmetric particle (LSP), as there is no dark matter constraint [34–36]. Furthermore, the LSP can possibly decay within the detector. Therefore, RPV scenarios entail a different and richer phenomenology of signatures [37, 38] than RPC. At this point, we note Wagner’s conjecture on signature anomalies at the LHC [39]. If it holds, it would state that a comprehensive coverage of new physics is possible with RPV searches, see also Refs. [36, 38, 40, 41]. We take this as a further motivation to investigate the broad range of RPV signatures in existing and planned experiments. Here, we focus specifically on signatures resulting from a light long-lived neutralino LSP,  $\tilde{\chi}_1^0$ .

Within the RPV scenarios, the lightest neutralino is the LSP in large regions of the RPV-MSSM parameter space [34, 36, 42–44]. Going beyond the RPV-MSSM and allowing for non-universal gaugino masses, the neutralino is still the LSP in large regions of parameter space, furthermore, it can be very light [45–47]. In fact, a massless neutralino is consistent with all laboratory and observational data [48–50]. We emphasize, a light neutralino in the MeV mass range cannot constitute the dark matter of the Universe, as it violates the Lee-Weinberg bound [51–56], it must decay.

A neutralino with mass lighter than a few GeV is necessarily dominantly bino-like [45, 49]. Thus, at tree-level, it does not couple to the  $Z^0$  boson and contributes only minimally to its invisible width [49]. Due to its small mass, such a light neutralino can be long-lived on collider experiment time scales, while decaying via RPV-induced interactions [8, 57, 58]. Such long-lived states are particularly interesting since their displaced or delayed signatures are less constrained by existing collider searches and may be more effectively probed at dedicated long-lived particle (LLP) experiments. We provide more details in Section 2. For a neutralino with mass  $m_{\tilde{\chi}_1^0} \lesssim \mathcal{O}(1 \text{ GeV})$ , the leading possible decay modes at tree-level are [59]

$$\tilde{\chi}_1^0 \rightarrow \begin{cases} \ell_i^+ \ell_k^- \nu_j, \nu_i \nu_j \nu_k, & L_i L_j \bar{E}_k, \\ \ell_i^\pm M_{jk}^\mp, \nu_i M_{jk}^0, & L_i Q_j \bar{D}_k, \\ p + M^-, n + M^0, \bar{U}_1 \bar{D}_1 \bar{D}_2. & \end{cases} \quad (1.1)$$

Here  $\ell_{i,k}^\pm \in \{e^\pm, \mu^\pm\}$  are light charged leptons, the  $\nu_{i,j,k}$  denote the 3 possible neutrinos, and we write  $M^{(0,\pm,')}$  for the various potential meson final states. In all cases the charge conjugate final state is also allowed, as the  $\tilde{\chi}_1^0$  is a Majorana fermion. On the right, we list the dominant RPV operator of the decay with generation indices.

In this paper, we focus on an interesting signature, which only arises at 1-loop order in RPV-SUSY. The neutralino can decay to just a neutrino and a photon via operators of the form  $L_i L_j \bar{E}_j$  or  $L_i Q_j \bar{D}_j$  [37, 60]

$$\tilde{\chi}_1^0 \rightarrow \gamma + \bar{\nu}_i^{(-)}. \quad (1.2)$$

This signature is also well-motivated by theories such as gauge-mediated supersymmetry breaking (GMSB) [61], extensions involving hidden or dark sectors that couple feebly to the SM [62], and models with universal extra dimensions [63]. In all these cases, the combination of high-energy photons with missing transverse energy provides a clean and experimentally robust probe of BSM dynamics, making it a key search channel at current and future collider experiments. This opens a new window for discovery.

Such final states have been extensively studied in context of ATLAS and CMS [64–69]. Ref. [70] investigates the capabilities of the FASER and FASER2 [71–73] detectors to look for such a signal using the simulation tool FORESEE within RPV-SUSY. However, many existing and proposed collider-based experiments are capable of probing such a signal, including FACET [74], MATHUSLA [75], CODEX-b [76, 77], ANUBIS [78], and MoEDAL-MAPP [79], which is in two phases: MAPP and MAPP2. Here we go beyond the work of Ref. [70] to investigate the signature Eq. (1.2) at the additional collider-based experiments listed above. We also go beyond the simulation technique of Ref. [70], which we describe in detail in Section 3. We thus investigate this search channel for a broad set of experiments using a different simulation method, and perform a comparative sensitivity study of these experiments under well motivated benchmark scenarios. Note, we restrict ourselves here to collider-based experiments. We leave a study of the single-photon signature at fixed-target experiments such as DUNE [80–83] and SHiP [84–86], or at neutrino reactor experiments such as JUNO [87] for a later study.

This paper is organised as follows. Section 2 provides the theoretical framework of the RPV-MSSM and the lightest neutralino in detail. The simulation strategy for the signal estimation is described in Section 3. The outcomes of the simulations performed for various experimental setups are presented in Section 4. Finally, Section 5 provides a summary of the results and concluding remarks.

## 2 Theoretical Framework

### 2.1 The RPV-MSSM

Given the particle content of the MSSM and the structure of the  $N = 1$  supersymmetry algebra, the most general renormalizable and  $SU(3)_C \times SU(2)_L \times U(1)_Y$ -invariant superpotential can be written as [42]

$$W = W_{\text{MSSM}} + W_{\text{LNV}} + W_{\text{BNV}}, \quad (2.1)$$

where  $W_{\text{MSSM}}$  is the usual MSSM superpotential, and, the RPV terms are given by

$$W_{\text{LNV}} = \frac{1}{2} \lambda_{ijk} L_i L_j \bar{E}_k + \lambda'_{ijk} L_i Q_j \bar{D}_k + \kappa_i H_u L_i, \quad W_{\text{BNV}} = \frac{1}{2} \lambda''_{ijk} \bar{U}_i \bar{D}_j \bar{D}_k. \quad (2.2)$$

The additional terms  $W_{\text{LNV}}$  and  $W_{\text{BNV}}$  introduce lepton-number-violating (LNV) and baryon-number-violating (BNV) interactions, respectively.  $L_i(Q_i)$  and  $\bar{E}_i(\bar{U}_i, \bar{D}_i)$  denote the lepton (quark)  $SU(2)_L$  doublets and  $SU(2)_L$  singlet chiral superfields, respectively.  $H_u$  is the up-type Higgs doublet. The indices  $i, j, k \in \{1, 2, 3\}$  represent generation indices with a summation implied over repeated indices. The  $\lambda, \lambda'$ , and  $\lambda''$  are dimensionless coupling constants. The  $\kappa_i$  are dimension-one mass mixing parameters. We shall set them to zero in our analysis. This corresponds to a basis choice [42, 43, 88–91]. We have suppressed gauge indices here.

While  $W_{\text{LNV}}$  and  $W_{\text{BNV}}$  are usually set to zero by imposing RPC to ensure proton stability, some RPV interactions may still be allowed if only specific terms are present [58, 91–94], or if the associated couplings are sufficiently small to satisfy experimental constraints [40, 41, 95–98]. In the following we shall consider non-zero values for the  $\lambda_{ijk}, \lambda'_{ijk}$  LNV couplings.

## 2.2 A Long-lived Light Neutralino

In RPV-SUSY, any SUSY particle can be the LSP [34–36, 99]. We shall consider the case of a neutralino LSP here. Neutrinos can be produced indirectly via the strong interaction via meson decays, *e.g.* pions:  $\pi^+ \rightarrow \mu^+ + \nu_\mu$ . Similarly neutralinos can also be singly produced, for example, via the decays of pseudoscalar mesons. This involves the  $LQ\bar{D}$  operators with  $\lambda'$  couplings. The corresponding decay widths are provided in Ref. [84], which we show here using the same conventions:

$$\Gamma(M_{ab} \rightarrow \tilde{\chi}_1^0 + l_i) = \frac{\lambda^{\frac{1}{2}}(m_{M_{ab}}^2, m_{\tilde{\chi}_1^0}^2, m_{l_i}^2)}{64\pi m_{M_{ab}}^3} |G_{iab}^{S,f}|^2 (f_{M_{ab}}^S)^2 (m_{M_{ab}}^2 - m_{\tilde{\chi}_1^0}^2 - m_{l_i}^2). \quad (2.3)$$

Here,  $l_i$  represents either a charged lepton  $\ell_i^\pm$  or a neutrino  $\nu_i$ , depending on whether the meson  $M_{ab}$  is charged or neutral. The  $G_{iab}^{S,f}$  are given in terms of linear combinations of various  $\lambda'/m_{\text{SUSY}}^2$ , where  $\lambda'$  is the RPV coupling involved in the production of the neutralino and  $m_{\text{SUSY}}$  is the mass of the SUSY particle mediating the decay [84].  $a, b$  are the generation indices of the quark/antiquark bound in the meson.  $m_{M_{ab}}, m_{\tilde{\chi}_1^0}$ , and  $m_{l_i}$  denote the meson, the neutralino and the lepton mass, respectively.  $\lambda^{\frac{1}{2}}(x, y, z) \equiv \sqrt{x^2 + y^2 + z^2 - 2xy - 2yz - 2xz}$  is the square root of the Källén function. The  $f_{M_{ab}}^S$  denote the pseudoscalar meson decay constants.

As mentioned, the lightest neutralino  $\tilde{\chi}_1^0$  can be very light, even massless [50]. Such a light neutralino with mass below about 1 GeV can decay via RPV interactions leading to so-called “displaced vertices”, if the RPV couplings are sufficiently small. The decay vertex can be displaced by meters or even 100s of meters [45, 46, 70, 100,

101]. Several dedicated far-detector programs have been proposed near the LHC interaction points (IPs), primarily designed to search for such long-lived particles (LLPs) with just such decay lengths on the order of  $c\tau \sim (1-100)$  m, or longer.

At loop level, the neutralino can decay radiatively to a photon and a neutrino through the  $W_{\text{LNV}}$  terms, as discussed in [60, 70, 90, 100], *cf.* Eq. (1.2). Since the final state consists of a photon accompanied by missing energy carried away by the neutrino, this decay channel offers a particularly clean signature with low backgrounds in experiments. In addition, it enables sensitivity to lower-mass neutralino scenarios that might otherwise be inaccessible, as the final state has effectively no mass threshold. The decay width of the process is

$$\Gamma(\tilde{\chi}_1^0 \rightarrow \gamma \nu_i^{(-)}) = \frac{\alpha^2 \lambda^{(\prime)2} m_{\tilde{\chi}_1^0}^3}{512\pi^3 \cos\theta_W} \left[ \sum_f e_f N_c m_f \frac{(4e_f + 1)}{m_{\tilde{f}}^2} \left( 1 + \log\left(\frac{m_f^2}{m_{\tilde{f}}^2}\right) \right) \right]^2, \quad (2.4)$$

where  $\lambda^{(\prime)}$  denotes the relevant RPV coupling which contributes to the process. Note, that these have to have the index structure:  $\lambda_{ijj}$  or  $\lambda'_{ijj}$ . The notation in Eq. (2.4) is the same as Ref. [70].  $e_f$ ,  $m_f(m_{\tilde{f}})$  and  $C_f$  are the electric charge, mass and the color factors ( $C_f = 3$  for quarks,  $C_f = 1$  for leptons) of the fermions (sfermions) in the loop, respectively.  $\alpha$  is the fine structure constant,  $\theta_W$  is the electroweak mixing angle. For the  $\lambda$  ( $LL\bar{E}$ ) coupling, the loop contains a  $\ell_i - \tilde{\ell}_i$  pair, where  $\ell$  is a charged lepton. For the  $\lambda'$  ( $LQ\bar{D}$ ) coupling, a  $d_i - \tilde{d}_i$  pair is required. In the decay width, the  $b$  quark gives the largest contribution in the  $\lambda'$  case due to its large mass, note the  $\sim m_f^2$  dependence. For the  $\lambda$  case, the  $\tau$  in the loop gives the highest contribution. A summary of upper bounds on the relevant RPV couplings used in this study is provided in Tab. 1, which are obtained from Ref. [36, 102].

$ijk$	$\lambda_{ijk}$	$\lambda'_{ijk}$
112	—	$0.21\left(\frac{m_{\tilde{s}_R}}{1\text{TeV}}\right)$
211	$0.49\left(\frac{m_{\tilde{c}_R}}{1\text{TeV}}\right)$	$0.59\left(\frac{m_{\tilde{d}_R}}{1\text{TeV}}\right)$
212	$0.49\left(\frac{m_{\tilde{\mu}_R}}{1\text{TeV}}\right)$	$0.59\left(\frac{m_{\tilde{s}_R}}{1\text{TeV}}\right)$
221	—	1.12
222	—	1.12
313	$0.019\left(\frac{m_{\tilde{\tau}}}{1\text{TeV}}\right)^{\frac{1}{2}}$	1.12
322	$0.70\left(\frac{m_{\tilde{\mu}_R}}{1\text{TeV}}\right)$	1.12
333	—	1.04

**Table 1:** Summary of current constraints of the  $\lambda_{ijk}$  ( $L_i L_j \bar{E}_k$ ) and  $\lambda'_{ijk}$  ( $L_i Q_j \bar{D}_k$ ) couplings [36, 102]. The selected generation indices  $ijk$  are present in the benchmarks investigated in Section 4.

Meson $M$	$\pi^\pm$	$\pi^0$	$K^\pm$	$K_L$	$K_S$
$N_M$	$1.64 \times 10^{19}$	$9.24 \times 10^{18}$	$2.38 \times 10^{18}$	$1.30 \times 10^{18}$	$1.31 \times 10^{18}$
Meson $M$	$D^\pm$	$D_s^\pm$	$B^\pm$	$B^0/\bar{B}^0$	
$N_M$	$2.03 \times 10^{16}$	$6.62 \times 10^{15}$	$1.46 \times 10^{15}$	$1.46 \times 10^{15}$	

**Table 2:** Number of mesons over the total  $4\pi$  solid angle produced in  $pp$  collisions at the LHC with a center-of-mass energy of 14 TeV and an integrated luminosity of  $3 \text{ ab}^{-1}$ . For Kaons,  $D$ - and  $B$ -mesons we follow Ref. [101, 103], while for pions we obtain  $N_M$  with the cross sections provided by FORESEE [104].<sup>1</sup>

### 3 Simulation Procedure

Within the light neutralino framework described in the previous section, we can estimate the number of observable neutralinos  $N_{\tilde{\chi}_1^0}^{\text{obs}}$  for various dedicated LLP detectors at the LHC. We begin by calculating the number of produced neutralinos via

$$N_{\tilde{\chi}_1^0, M_{ab}, X} = N_{M_{ab}} \cdot \text{Br}(M_{ab} \rightarrow \tilde{\chi}_1^0 + X), \quad (3.1)$$

where  $N_{M_{ab}}$  is the number of mesons  $M_{ab}$  (see Table 2) expected to be produced at the LHC during the runtime of the detector and  $\text{Br}(M_{ab} \rightarrow \tilde{\chi}_1^0 + X)$  is the branching ratio of a meson  $M_{ab}$  to decay into a neutralino and other final state particles  $X$ , *cf.* Eq. (2.3). If the neutralinos are sufficiently long-lived, they travel a macroscopic distance and decay with an average probability  $\langle P(\tilde{\chi}_1^0 \text{ in f.v.}) \rangle_{M_{ab}, X}$  in the fiducial volume of the detector being considered. As we are specifically interested in the photon signature of the neutralino, *cf.* Eq. (2.4), we obtain  $N_{\tilde{\chi}_1^0}^{\text{obs}}$  by

$$N_{\tilde{\chi}_1^0}^{\text{obs}} = \text{Br}(\tilde{\chi}_1^0 \rightarrow \gamma + \nu_i^{(-)}) \cdot \sum_{M_{ab}, X} N_{\tilde{\chi}_1^0, M_{ab}, X} \cdot \langle P(\tilde{\chi}_1^0 \text{ in f.v.}) \rangle_{M_{ab}, X}. \quad (3.2)$$

In order to estimate the average decay probability, we employ Monte-Carlo techniques. The probability of any neutralino to decay inside of a reference volume can be obtained using the exponential decay law

$$P_i(\tilde{\chi}_1^0 \text{ in f.v.}) = \exp\left(-\frac{L_{T,i}}{\lambda_i}\right) \left[1 - \exp\left(-\frac{L_{I,i}}{\lambda_i}\right)\right], \quad (3.3)$$

where  $L_{T,i}$  is the length the neutralino travels from its production vertex to the detector volume and  $L_{I,i}$  is the length it would travel inside the detector volume if it would not decay.  $L_{I,i}$  takes into account the flight direction of the neutralino, as

<sup>1</sup>Our approach goes beyond the implementation using FORESEE in the simulation of proton-proton events. While the event generation is performed using `Pythia 8.313`, we employ meson-production inputs consistent with those used in FORESEE. In particular, the pion and kaon production numbers are based on cross sections obtained with `EPOS-LHC`.

well as the extent of the detector being considered along that axis.  $\lambda_i$  is the boosted decay length, which is determined by the Lorentz factor  $\gamma_i$ , the speed  $\beta_i$  and the total decay rate of the neutralino

$$\lambda_i = \gamma_i \beta_i \tau_{\tilde{\chi}_1^0} = \frac{\gamma_i \beta_i}{\Gamma_{\text{tot}, \tilde{\chi}_1^0}}. \quad (3.4)$$

Simulating  $N_{M_{ab}, X}^{\text{MC}}$  neutralinos for each production mode, the average decay probability is given by

$$\langle P(\tilde{\chi}_1^0 \text{ in f.v.}) \rangle_{M_{ab}, X} = \frac{1}{N_{M_{ab}, X}^{\text{MC}}} \sum_i^{N_{M_{ab}, X}^{\text{MC}}} P_i(\tilde{\chi}_1^0 \text{ in f.v.}). \quad (3.5)$$

We note here, that the average decay probability has to be evaluated individually for each decay mode  $M \rightarrow \tilde{\chi}_1^0 + X$ , since the kinematic variables depend on the masses of the involved particles and the number of particles involved. If we were to average only for the  $\tilde{\chi}_1^0$  or average the probability for each initial meson  $M$ , we might overestimate  $\langle P \rangle$  by combining a large decay rate for one mode  $X_1$  with a high decay probability of another mode  $X_2$ .

We use the event generator `Pythia 8.313` [105] to simulate  $10^6$  proton-proton collisions with a center-of-mass energy of 14 TeV. Depending on the considered initial mesons  $M_{ab}$ , we activate the modules “`SoftQCD:a11`” ( $\pi, K$ ),<sup>2</sup> “`HardQCD:hardccbar`” ( $D, D_s$ ) or “`HardQCD:hardbbbar`” ( $B$ ). We let the mesons decay into a neutralino and some final state  $X$ . In order to improve statistics, we only allow for decays into a neutralino during the event generation and correct for the branching ratio after the simulation.

The lengths  $L_{T,i}$  and  $L_{I,i}$  are calculated employing the algorithm described in Ref. [101], using the  $\tilde{\chi}_1^0$  production vertex and the detector geometries. In addition to `FASER` and `FASER2` [107, 108], for which the single photon signature was already investigated in Ref. [70] using `FORESEE` [104] for event generation, here we also analyze the potential for this signature at `ANUBIS` [78, 109], `CODEX-b` [76, 110, 111], `FACET` [74], `MAPP`, `MAPP2` [79, 112, 113] and `MATHUSLA` [114–117]. We simply compute event rates and assume that these experiments are able to detect the photon plus missing energy signature of the neutralino decay. The implemented geometry for most detectors is described in Ref. [103].<sup>3</sup>

---

<sup>2</sup>Pythia is generally tuned for the central region of the LHC. The production of some particles such as  $\pi^0$  is not well validated for  $\eta > 5$ . We account for this by following the far-forward tuning described in Ref. [106] when investigating pions as initial mesons.

<sup>3</sup>The geometry of `ANUBIS` is still subject to change. Ref. [78] proposed using the `PX14` access shaft above `ATLAS` as a detection volume by lining the shaft with four 1 m thick tracking stations at 18.5 m intervals. Currently, the preferred configuration is lining the ceiling of the `ATLAS` cavern `UX15` with these tracking stations to enhance the covered solid angle. As the ceiling configuration

Category	Veto Conditions	Initial Meson	Applied to
Hadron Calorimetry (ATLAS)	$\rho \leq 2.28$ m $z \leq 4.277$ m	All	ANUBIS
Hadron Calorimetry (ATLAS)	$\rho \leq 1.77$ m $z \leq 4.0$ m	All	MATHUSLA
TAN (IR1 / IR5) TAS (IR1 / IR5)	$z \leq 141.2$ m $z \leq 19.05$ m	Neutral Mesons Charged Mesons	FASER, FACET
Shield Veto	$\rho \leq 5.0$ m $z \leq 3.0$ m	All	CODEX-b
Cavern Wall	$\rho \leq 1.9$ m	All	MAPP, MAPP2

**Table 3:** Summary of the vetos of Ref. [101] implemented in the Monte Carlo simulation.

An important difference between the event generation we employ here compared to that used in Ref. [70] is that `Pythia 8.313` simulates actual decay vertices of the initial mesons. If  $M_{ab}$  is long-lived, it decays a macroscopic distance away from the interaction point, which affects the distances  $L_{T,i}$  and  $L_{I,i}$ . Additionally, we veto neutralino events depending on the macroscopic distance traveled by the meson, as described in Ref. [101]. The displaced decay vertices together with the veto conditions affect the momentum spectrum of the neutralino we consider for the average decay probability and hence also  $N_{\tilde{\chi}_1^0}^{\text{obs}}$ . We summarize the veto categories in Table 3.

## 4 Results

In this section, we present the results of our simulations for the six benchmarks proposed in Ref. [70]. We summarize key characteristics of them in Table 4.

### 4.1 Benchmark 1

For the first benchmark we assume only  $\lambda'_{211}$  and  $\lambda'_{333}$  to be non-zero. The former coupling induces the decays  $\pi^\pm \rightarrow \tilde{\chi}_1^0 + \mu^\pm$  and  $\pi^0 \rightarrow \tilde{\chi}_1^0 + \nu_\mu$ , while both couplings allow for a radiative decay of the neutralino via either a  $d$ - or a  $b$ -quark loop. Since the radiative decay of the neutralino is proportional to  $m_f^2$ , where  $m_f$  is the mass of the fermion in the loop, *cf.* Eq. (2.4), we allow for a non-zero  $\lambda'_{333}$  in addition to  $\lambda'_{211}$  to enhance the decay rate of the neutralino. We neglect contributions from

---

is not yet finalised, we approximated the detection volume using a segment of a tube with an inner radius of 20 m, a height of 45 m and an azimuthal angle coverage of  $60^\circ$ .

For MATHUSLA, the decay volume has been significantly reduced compared to what was assumed in Ref. [103] (see Ref. [117] for the current status), while the decay volume of MAPP2 has been extended to cover a greater part of the UGC1 gallery. MAPP has been moved from the UGC1 gallery to the UA83 tunnel about 100 m from IP8.

Benchmark	$\lambda_{P,iab}$	$M_{ab}$	$\lambda_{D,i'j'j'}$	$\gamma$ -signature
<b>B1</b>	$\lambda'_{211}$	$\pi^\pm, \pi^0$	$\lambda'_{333}$	$\gamma + \nu_\mu$ ( $d$ ), $\gamma + \nu_\tau$ ( $b$ )
<b>B2</b>	$\lambda'_{212}$	$K^\pm, K_{L/S}$	$\lambda'_{333}$	$\gamma + \nu_\tau$ ( $b$ )
<b>B3</b>	$\lambda'_{112}$	$K^\pm, K_{L/S}$	$\lambda_{322}$	$\gamma + \nu_\tau$ ( $\mu$ )
<b>B4</b>	$\lambda'_{221}$	$D^\pm, K_{L/S}$	$\lambda_{233}$	$\gamma + \nu_\mu$ ( $\tau$ )
<b>B5</b>	$\lambda'_{222}$	$D_s^\pm$	$\lambda'_{222}$	$\gamma + \nu_\mu$ ( $s$ )
<b>B6</b>	$\lambda'_{313}$	$B^\pm, B^0$	$\lambda'_{333}$	$\gamma + \nu_\tau$ ( $b$ )

**Table 4:** Summary of the benchmarks proposed in Ref. [70]. We list the non-zero couplings, the related mesons decaying into the neutralino, and the decays of neutralinos into the photon signature. In brackets, we signalize the fermion that is involved in the loop in the photon decay. See the respective subsections for more detail.

$\rho$  ( $\Upsilon$ ) mesons decaying into neutralinos via a non-zero  $\lambda'_{211}$  ( $\lambda'_{333}$ ). As discussed in Ref. [84], the lifetime of vector mesons is typically several orders of magnitude shorter than those of pseudoscalar mesons, so that the branching ratio of vector mesons into neutralinos and thus the production of neutralinos from vector mesons decays is negligible. Additionally, the production rate of  $\Upsilon$  mesons at the LHC is significantly lower compared to lighter mesons, enhancing the suppression. Hence, we omit these production channels from our simulation.

We are interested in a benchmark involving the production of the light neutralinos via pions, since the latter are abundantly produced at the LHC. We note however, that the relatively large muon mass restricts the kinematically available mass range for the neutralinos produced in  $\pi^\pm$  decays, while the branching ratio of  $\pi^0$  into neutralinos is diminished due to the short lifetime of  $\pi^0$ . We could increase the neutralino mass range in charged decays by considering electrons and a non-zero  $\lambda'_{111}$ , but this coupling is heavily restricted from neutrinoless double beta decay searches [102, 118, 119].

We present the results of the simulation in the  $\lambda'/m_{\text{SUSY}}^2$  vs.  $m_{\tilde{\chi}_1^0}$  plane in Fig. 1 as 3-event isocurves, which correspond to a 95% C.L. exclusion limit assuming no observation and no background events. We assume the coupling strengths of the non-zero couplings to be equal. The results of Ref. [70] for **FASER** and **FASER2** are included as dotted lines and the already excluded region for the couplings is marked as a gray area. Assuming mass degenerate sfermions with  $m_{\text{SUSY}} = 1$  TeV, we have taken the stronger constraint listed in Table 1 into account.

In Fig. 1, we can see that all detectors follow a similar pattern. Up to  $m_{\tilde{\chi}_1^0}^{\text{th}} \approx 35$  MeV, the isocurves expand beyond already excluded areas, where the extent seems to favor larger neutralino masses. We can group the isocurves for all detectors as **ANUBIS** and **MATHUSLA** having the greatest sensitivity reach down to  $\lambda'/m^2 \approx 7.5 \times 10^{-9}$  GeV $^{-2}$ , followed by **CODEX-b**, **FACET** and **MAPP2**. **FASER2** can

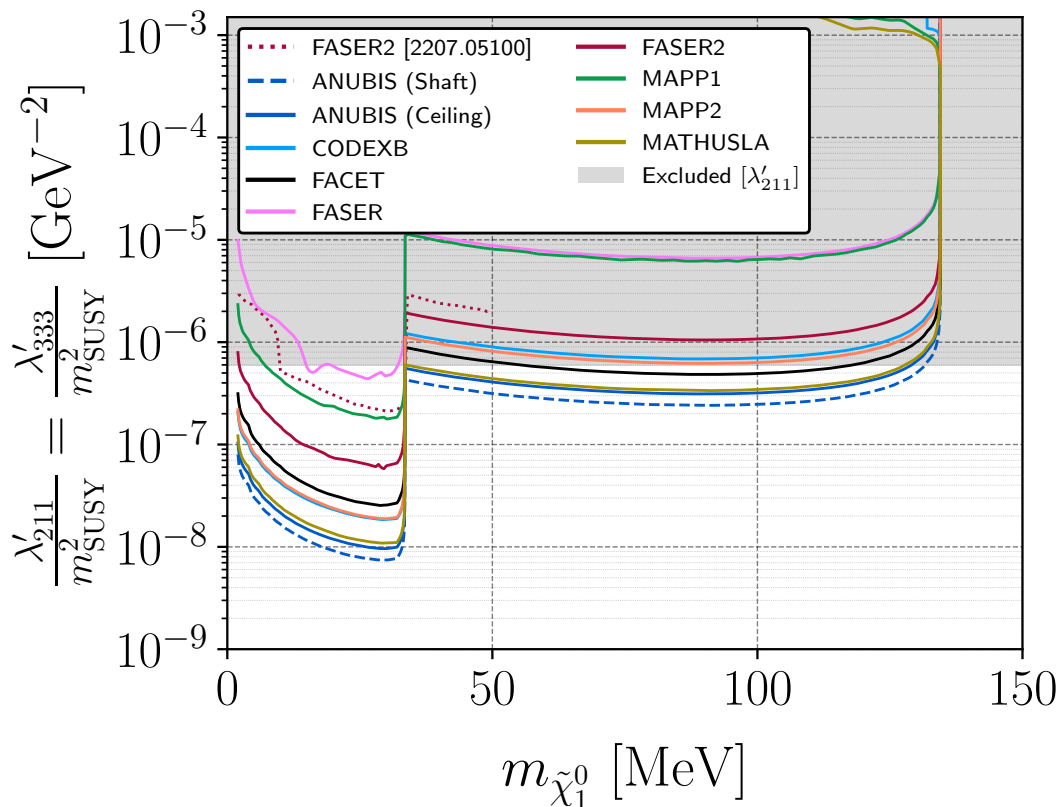


**Figure 1:** 3-event isocurves in the  $\lambda/m_{\text{SUSY}}^2$  vs.  $m_{\tilde{\chi}_1^0}$  plane for benchmark 1. We assume mass degenerate sfermions and equal coupling strengths for  $\lambda'_{211}$  and  $\lambda'_{333}$ . Previous results from Ref. [70] are presented as dotted lines. The gray shaded area represents already excluded coupling regions, where the constraint for  $\lambda'_{211}$  is the strongest constraint assuming  $m_{\text{SUSY}} = 1$  TeV.

reach coupling strengths above  $6 \times 10^{-8} \text{ GeV}^{-2}$ , while MAPP and FASER are barely sensitive below the existing coupling bound.<sup>4</sup>

The relative sensitivity reach between the detectors is determined by the considered integrated luminosity, the covered solid angle, the fiducial volume, as well as the location of the detectors and the associated veto conditions. In this mass region, the main contribution to the observed events is from charged pion decays. These decays are prohibited for  $m_{\tilde{\chi}_1^0} > m_{\tilde{\chi}_1^0}^{\text{th}}$ , so that only a couple of the detectors, namely

<sup>4</sup>Some isocurves manifest fluctuations in the sensitivity reach, e.g. FASER, FASER2 and MAPP. These are not physical, but rather due to limited statistics. These detector concepts are located furthest from the interaction vertex and cover only a small solid angle. Thus, the event rates are naturally small, requiring higher statistics for precise results. A similar effect can be observed in the small decay length (large coupling) limit for all detectors. In this limit, neutralinos require a large boost to sufficiently contribute to  $\langle P \rangle$  and not decay before reaching the detector. Since the limit is already excluded by existing coupling constraints for all benchmarks, we do not address this issue by increasing the amount of simulated  $pp$  collisions.

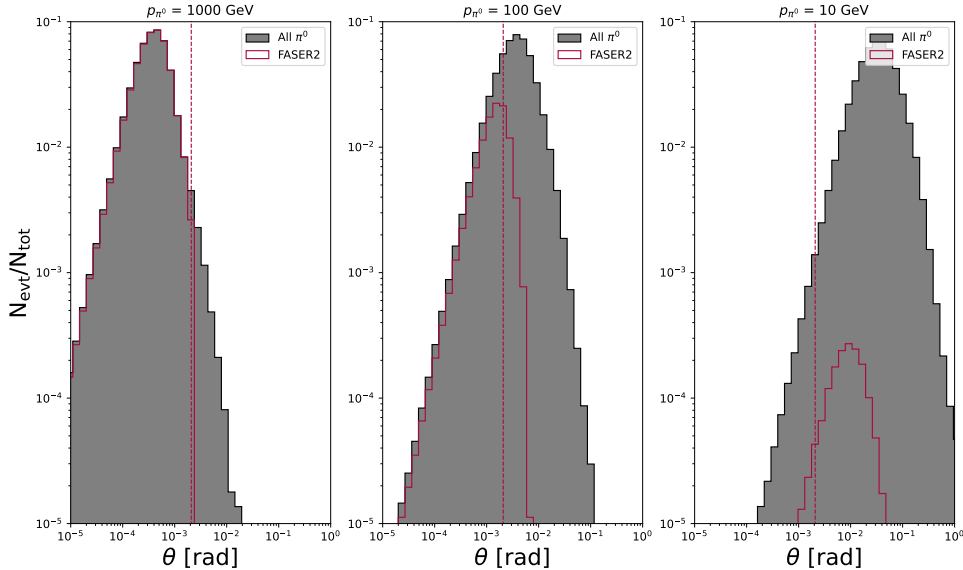


**Figure 2:** Normalized  $\theta$ -distributions of neutral pions generated in  $N_{\text{MC}} = 10^6$  14 TeV  $pp$  events using the `SoftQCD` module of Pythia with the Forward Physics Tune [106] for  $p_{\pi^0} = 1000$  GeV (left), 100 GeV (middle) and 10 GeV (right).  $\theta$  is the angle of the pion momentum with respect to the beam axis. The neutralino mass is set to  $m_{\tilde{\chi}_1^0} = 20$  MeV. The gray histogram represents the  $\theta$ -distribution of all  $\pi^0$ , while the red histogram denotes the  $\theta$ -distribution within FASER2. The red vertical dashed line depicts the angular acceptance of FASER2.

ANUBIS, MATHUSLA and for some mass regions FACET, can reach coupling regions beyond existing limits.

The sensitivity reach of FASER2 in our simulation is enhanced compared to previous results of Ref. [70]. However, the dotted and solid isocurve are closer aligned for  $m_{\tilde{\chi}_1^0} > m_{\tilde{\chi}_1^0}^{\text{th}}$ , while they differ more significantly for  $m_{\tilde{\chi}_1^0} < m_{\tilde{\chi}_1^0}^{\text{th}}$ . In Ref. [70], FORESEE was used for event generation, where effects of long-lived initial mesons are taken into account by applying the exponential decay law to the decay probability. The exact decay position is not simulated and vetos based on the decay position were not included. Since here we do include the exact decay position, the detector sensitivity is affected in several ways, which we now briefly discuss.

Firstly, mesons produced outside the geometric acceptance of FASER2 can nevertheless decay into neutralinos that propagate towards the detector. To illustrate this phenomenon, Fig. 2 depicts the normalized  $\theta$ -distributions of neutral pions. These have been generated in  $N_{\text{MC}} = 10^6$  14 TeV  $pp$  events using the `SoftQCD` module of Pythia with the Forward Physics Tune [106].  $\theta$  is the angle of the pion momenta with respect to the beam axis. For the momenta  $p_{\pi^0} = 1000$  GeV, 100 GeV and 10 GeV, we show the  $\theta$  distribution of all pions (gray) together with that of pions decaying into neutralinos that yield a non-zero contribution to  $\langle P \rangle$  for each detector (red). The

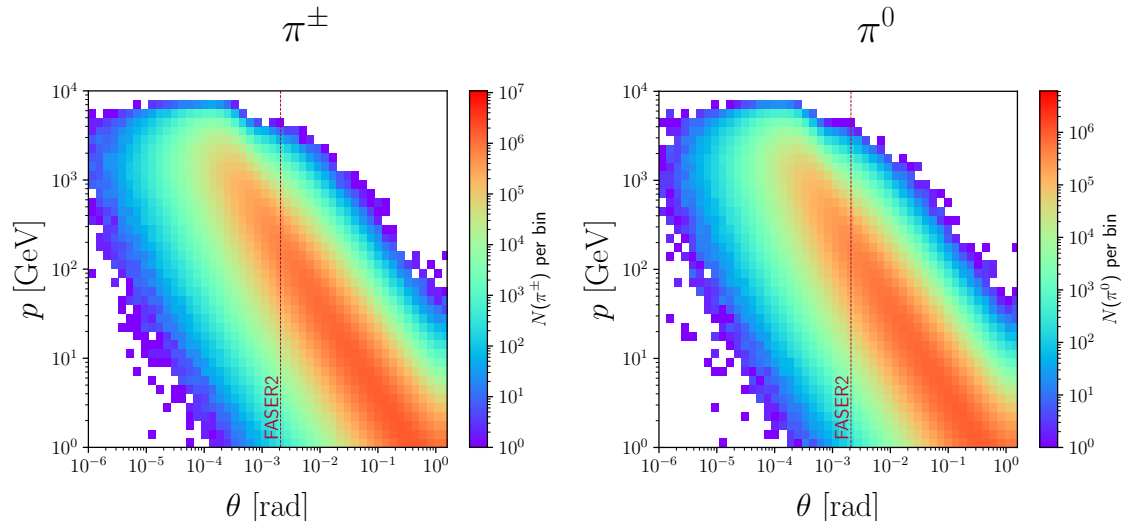


**Figure 3:**  $(\theta, p)$ -distribution of charged (left) and neutral (right) pions for  $N_{\text{MC}} = 10^6$  14 TeV  $pp$  events which have been generated using the `SoftQCD` module of Pythia with the Forward Physics Tune [106]. Here,  $p$  is the absolute value of the momentum and  $\theta$  is the angle of the pion momentum with respect to the beam axis. The red vertical dashed lines depict the angular acceptance of FASER2.

geometric acceptance of FASER2 is included as a red dashed vertical line. Especially at lower momenta, mesons outside the geometric acceptance contribute to the average decay probability. FORESEE partially accounts for this effect by incorporating the kinematics of the neutralino, while assuming the production vertex coincides with the interaction point. We see that allowing for a production vertex displaced from the interaction point, for instance closer to the detector, can additionally enhance the effective geometric acceptance.

Secondly, neutralinos produced at larger  $\theta$  exhibit a momentum spectrum shifted toward lower values than those originating in the far forward region (see Fig. 3 for the pion distributions). As demonstrated in Ref. [120], in the large decay length limit, *i.e.* the small coupling limit, we can approximate the average decay probability from Eq. (3.5) to first order as

$$\langle P(\tilde{\chi}_1^0 \text{ in f.v.}) \rangle_{M_{ab}, X} \approx \frac{1}{N_{M_{ab}, X}^{\text{MC}}} \sum_i^{N_{M_{ab}, X}^{\text{MC}}} \frac{L_{I,i}}{\lambda_i} = \frac{\Gamma_{\text{tot}, \tilde{\chi}_1^0}}{N_{M_{ab}, X}^{\text{MC}}} \sum_i^{N_{M_{ab}, X}^{\text{MC}}} \frac{L_{I,i}}{\gamma_i \beta_i}. \quad (4.1)$$

We see, that a modified momentum spectrum alters  $\langle P \rangle$ , as it is inversely proportional to the kinematic variables  $\gamma_i$  and  $\beta_i$ . A lower average momentum increases the average decay probability in this limit. Hence, the sensitivity of FASER2 is enhanced not only by the increased neutralino flux towards the detector, but also by the kinematic properties of the additional particles.

Lastly,  $\langle P \rangle$  is modified by the application of the veto conditions. For **FASER2** for instance, the TAS (TAN) absorber, located 19.05 m (141.2 m) downstream of the interaction point, restricts the allowed displaced decay vertices for charged (neutral) mesons. Neglecting the decay position relative to the surrounding infrastructure may therefore lead to an overestimate of the effective acceptance, particularly for highly boosted mesons decaying further away from the interaction point. In the large decay length limit, mesons and subsequent neutralinos with large momenta contribute less to the average decay probability [see Eq. (4.1)]. Overestimating the flux of high momenta neutralinos due to missing veto conditions does not compensate for the underestimation of low momenta neutralinos.

Thus, accounting for spatially displaced meson decay vertices at **FASER2** enhances the detector sensitivity in scenarios with long-lived mesons producing neutralinos sufficiently displaced from the interaction point. Since  $\tau_{\pi^\pm} \gg \tau_{\pi^0}$ , charged pions typically decay farther from the interaction point, enhancing the impact of displaced meson decay vertices in  $\pi^\pm$ -dominated regions with  $m_{\tilde{\chi}_1^0} < m_{\tilde{\chi}_1^0}^{\text{th}}$ .

The enhancing effect manifests itself further when comparing the relative ordering of **CODEX-b**, **FACET**, and **MAPP2** above and below  $m_{\tilde{\chi}_1^0}^{\text{th}}$  in Fig. 1. For  $m_{\tilde{\chi}_1^0} > m_{\tilde{\chi}_1^0}^{\text{th}}$ , the largest sensitivity reach is achieved by **FACET**, followed by **MAPP2** and **CODEX-b**. However, for  $m_{\tilde{\chi}_1^0} < m_{\tilde{\chi}_1^0}^{\text{th}}$ , where long-lived  $\pi^\pm$  dominate neutralino production, **MAPP2** and **CODEX-b** exhibit nearly identical sensitivities, whereas **FACET** becomes less sensitive to RPV couplings. While **FACET**, similar to **FASER2**, is positioned in the far-forward region, **CODEX-b** is located at the largest angle with respect to the beam axis of the three proposals. The sensitivity enhancement from displaced decays of long-lived  $\pi^\pm$  increases with larger  $\theta$  due to the shift of the meson momentum spectrum towards lower values.  $\pi^0$  mesons are comparatively short-lived, leading to a lesser enhancement due to displaced decays. As a result, the difference between the regions below and above  $m_{\tilde{\chi}_1^0}^{\text{th}}$  is amplified at larger  $\theta$  compared to the far-forward region, giving rise to the observed detector ordering.

## 4.2 Benchmark 2

For the second benchmark, we investigate neutralinos produced by kaon decays instead of pions. Hence, we consider  $\lambda'_{212}$  as the non-zero production coupling, while  $\lambda'_{333}$  induces the radiative decay. The neutralino is now produced via  $K^\pm \rightarrow \tilde{\chi}_1^0 + \mu^\pm$  and  $K_{L/S} \rightarrow \tilde{\chi}_1^0 + \nu_\mu$ . The radiative decay via a  $d$ -quark loop is not possible in this benchmark.

As for benchmark 1, we here present the results in Fig. 4 as 3-signal event isocurves assuming no background events. We include previous results as dotted lines and current coupling constraints as the gray area. The isocurves follow a similar structure for all detectors. The  $m_{\tilde{\chi}_1^0}$  reach is bounded from above by the kaon mass. We observe a small kink at masses below 400 MeV, where the neutralino production via the decay of charged kaons is kinematically available. We furthermore observe

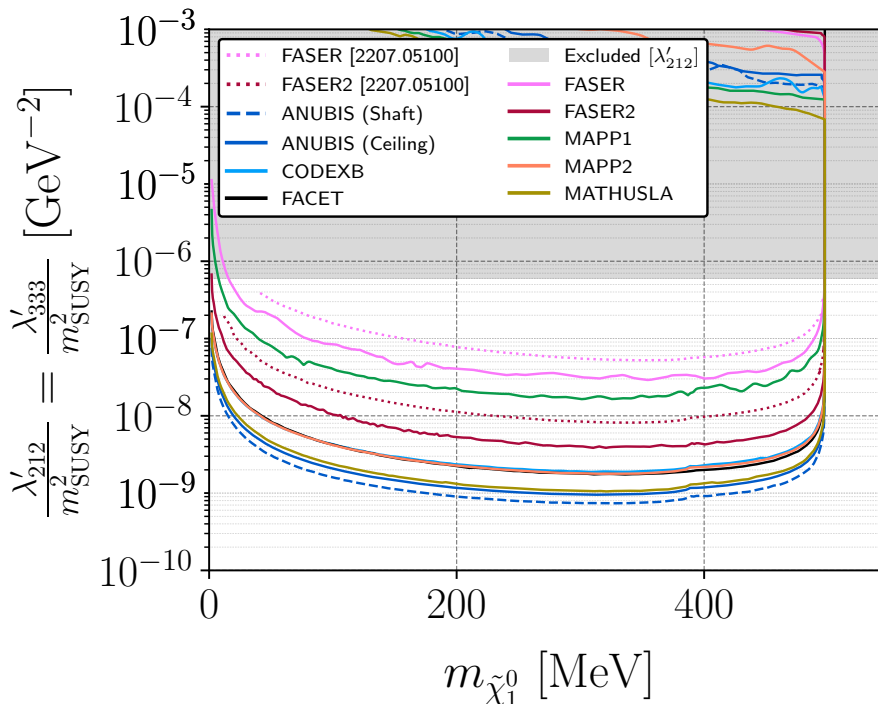


**Figure 4:** 3-event isocurves in the  $\lambda'/m_{\text{SUSY}}^2$  vs.  $m_{\tilde{\chi}_1^0}$  plane for benchmark 2. We assume mass degenerate sfermions and equal coupling strengths for  $\lambda'_{212}$  and  $\lambda'_{333}$ . Previous results from Ref. [70] are presented as dotted lines. The gray shaded area represents already excluded coupling regions, where the constraint for  $\lambda'_{212}$  is the strongest constraint assuming  $m_{\text{SUSY}} = 1 \text{ TeV}$ .

a slight asymmetry around the point of maximum sensitivity, with an increased sensitivity towards higher masses  $m_{\tilde{\chi}_1^0}$ . The maximum sensitivity is observed for  $m_{\tilde{\chi}_1^0} \approx 350 \text{ MeV}$  with  $\lambda'/m^2 \approx 7.5 \times 10^{-10} \text{ GeV}^{-2}$  for ANUBIS. The various detectors can be grouped as in benchmark 1, where ANUBIS and MATHUSLA show the greatest sensitivity, followed by CODEX-b, FACET and MAPP2, then FASER2, and finally MAPP and FASER show the lowest sensitivity.

We can also observe the effects of displaced kaon decays when comparing the results of our simulation with the previous investigation using FORESEE. As  $K^\pm$  and  $K_L$  are long-lived, the difference between both investigation can be explained as in benchmark 1. The neutralino momentum spectrum and the neutralino flux are modified by considering the explicit kaon decay vertices and the associated veto conditions in a way to enhance  $\langle P \rangle$ .

### 4.3 Benchmark 3

In this benchmark we select  $\lambda'_{112} \neq 0$  for the production of the neutralinos via kaon decays:

$$K^\pm \rightarrow \tilde{\chi}_1^0 + e^\pm, \quad K^0 \rightarrow \tilde{\chi}_1^0 + \nu_e. \quad (4.2)$$

For the neutralino decay we consider  $\lambda_{322} \neq 0$ . Leading to the radiative and tree-level decays

$$\tilde{\chi}_1^0 \rightarrow \begin{cases} \nu_\tau + \gamma, \text{ via a } (\mu - \tilde{\mu})\text{-loop,} \\ \nu_\tau + \mu^\pm + \mu^\mp. \end{cases} \quad (4.3)$$

For production via kaons the tree-level decay  $\tilde{\chi}_1^0 \rightarrow \nu_\mu + \tau^\pm + \mu^\mp$  is kinematically not possible. The additional neutralino decays reduce the branching fraction for the radiative decays.

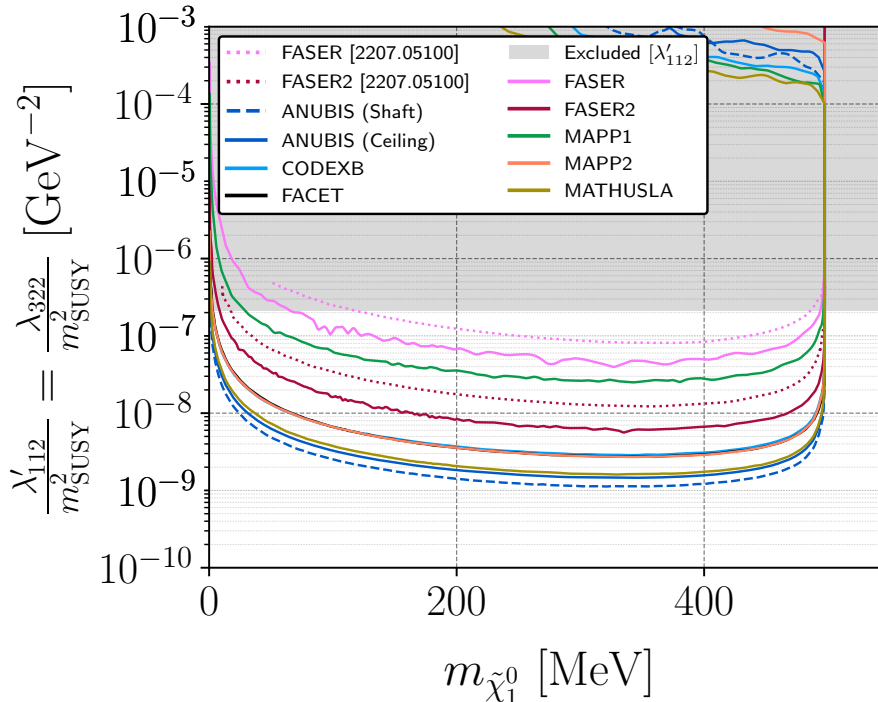


**Figure 5:** 3-event isocurves in the  $\lambda^{(l)}/m_{\text{SUSY}}^2$  vs.  $m_{\tilde{\chi}_1^0}$  plane for benchmark 3. We assume mass degenerate sfermions and equal coupling strengths for  $\lambda'_{112}$  and  $\lambda_{322}$ . Previous results from Ref. [70] for FASER/FASER2 are presented as dotted lines. The gray shaded area represents already excluded coupling regions, where the constraint for  $\lambda'_{112}$  is the strongest constraint assuming  $m_{\text{SUSY}} = 1$  TeV.

Results for benchmark 3 (Fig. 5) are very similar to benchmark 2 although overall the sensitivity is lower. The kink for masses below 400 MeV can no longer be observed, as the charged decays are already kinematically available, but we still observe the enhanced sensitivity for large  $m_{\tilde{\chi}_1^0}$ . The most sensitive detector is ANUBIS with a reach of  $\lambda'/m^2 \approx 10^{-9} \text{ GeV}^{-2}$ , while MAPP and FASER are the least sensitive. We can also observe the effects of the displaced decays, when comparing to previous results.

#### 4.4 Benchmark 4

To investigate heavier neutralinos, we now consider charm meson decays with a non-zero  $\lambda'_{221}$ . This coupling allows for the production of the neutralinos via the decay  $D^\pm \rightarrow \tilde{\chi}_1^0 + \mu^\pm$ , as well as via the neutral kaon decays  $K_{L/S} \rightarrow \tilde{\chi}_1^0 + \nu_\mu$ . This implies  $m_{\tilde{\chi}_1^0} < m_\tau$ . If the neutralino is heavy enough the latter production mode becomes kinematically inaccessible, but neutralino decays into kaons such as  $\tilde{\chi}_1^0 \rightarrow K_{L/S} + \nu_\mu$  and  $\tilde{\chi}_1^0 \rightarrow K^{*0} + \nu_\mu$  become allowed. For  $m_{\tilde{\chi}_1^0} > \mathcal{O}(1.5 \text{ GeV})$ , decays involving multi-meson final states might become relevant, but are neglected here for simplicity. As can be seen in Eq. (4.1), a larger total decay rate can increase the average decay probability, while it would reduce the branching ratio into the signature single- $\gamma$  decay. Quantifying this effect requires a detailed analysis, which goes beyond the scope of the present work. For the radiative decay, we again consider an  $LL\bar{E}$  coupling,  $\lambda_{233}$ , where the loop is mediated by a  $\tau - \tilde{\tau}$  pair. Fully leptonic decays are not possible because they always include at least one  $\tau$  and  $m_{\tilde{\chi}_1^0} < m_\tau$  for all available neutralino production modes.

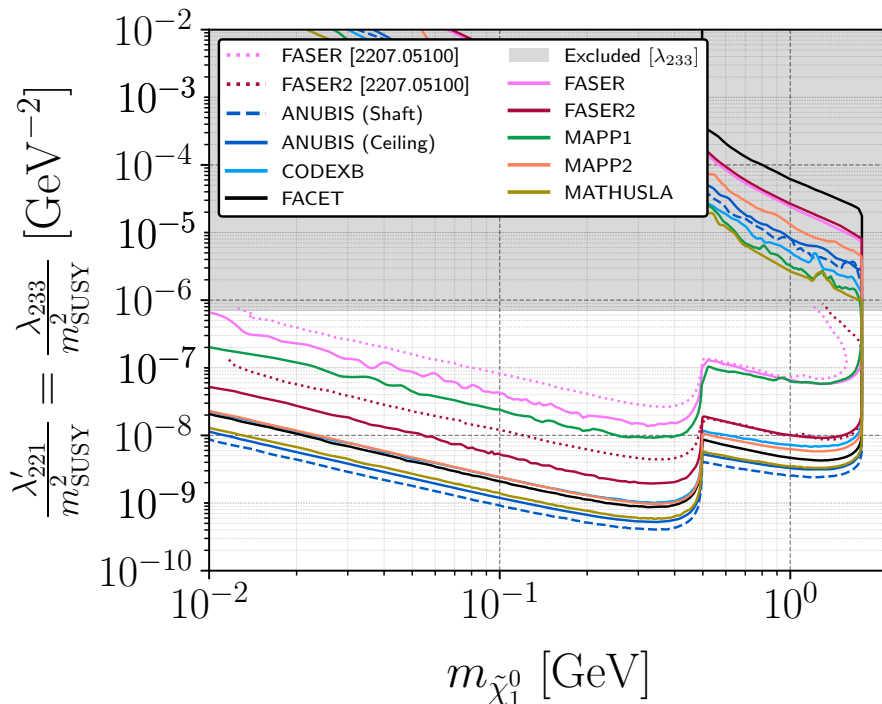


**Figure 6:** 3-event isocurves in the  $\lambda/m_{\text{SUSY}}^2$  vs.  $m_{\tilde{\chi}_1^0}$  plane for benchmark 4. We assume mass degenerate sfermions and equal coupling strengths for  $\lambda'_{221}$  and  $\lambda_{233}$ . Previous results from Ref. [70] are presented as dotted lines. The gray shaded area represents already excluded coupling regions, where the constraint for  $\lambda_{233}$  is the strongest constraint assuming  $m_{\text{SUSY}} = 1 \text{ TeV}$ .

We have chosen to depict the results of benchmark 4 (Fig. 6) as a function of

the logarithm of  $m_{\tilde{\chi}_1^0}$ . We can divide the sensitivity reach into  $m_{\tilde{\chi}_1^0}$ -regions where the production is dominated by kaon decays and  $m_{\tilde{\chi}_1^0}$ -regions where it can kinematically only proceed via the decay of charm mesons. As charm mesons are less abundantly produced at the LHC, the detectors are less sensitive to RPV couplings in the latter case. As expected from the previous benchmarks, ANUBIS is the most sensitive detector concept reaching couplings as low as  $\lambda'/m^2 \approx 4 \times 10^{-10} \text{ GeV}^{-2}$ , while the other detector concepts align as in previous benchmarks.

Comparing the isocurves for FASER and FASER2 with previous investigation, we see an enhanced sensitivity in our results for  $m_{\tilde{\chi}_1^0} < 500 \text{ MeV}$ . However, the curves agree for heavier neutralinos. Recall, we have an improved simulation procedure. Charm mesons decay promptly, so that the meson decay vertices are almost identical to the interaction point when considering macroscopic scales. Hence, the considered neutralino spectrum and our event generation is similar to Ref. [70].

#### 4.5 Benchmark 5

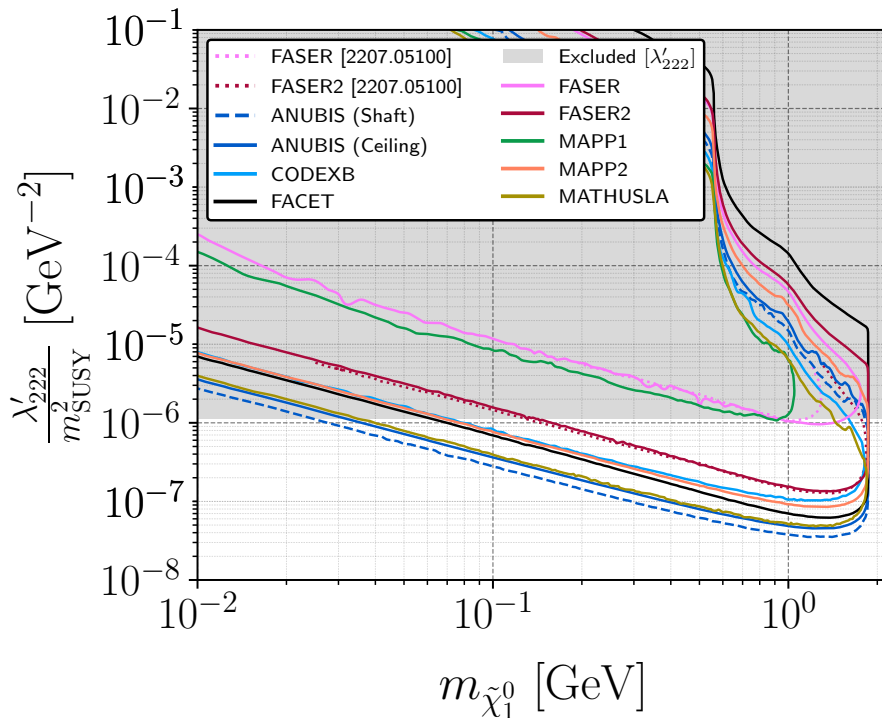
In benchmark five, we only consider a single non-zero coupling  $\lambda'_{222}$ . This coupling induces the production of the neutralinos via the decay  $D_s^\pm \rightarrow \tilde{\chi}_1^0 + \mu^\pm$  as well as the decay via the radiative mode  $\tilde{\chi}_1^0 \rightarrow \gamma + \nu_\mu$  via an s-quark loop. Additionally, the neutralino can decay into  $\eta$ ,  $\eta'$ , or  $\phi$  for a large enough  $m_{\tilde{\chi}_1^0}$ .

Fig. 7 displays the resulting 3-event isocurves. We can observe various features also present in the other benchmarks such as the order of sensitivity between the detectors. ANUBIS has the greatest sensitivity reach with  $\lambda'/m^2 \approx 3.5 \times 10^{-8} \text{ GeV}^{-2}$ , whereas MAPP and FASER2 are only sensitive up to existing limits. Since the  $D_s^\pm$  decay promptly, we do not observe the effects of displaced meson decays on the neutralino spectrum, so that our simulation results agree with Ref. [70]. Decays of the neutralinos into  $\eta$ ,  $\eta'$ , or  $\phi$  do not affect the shape of the isocurves for small couplings, while they influence the small decay length limit. Mass thresholds of these mesons can be observed in the already excluded regions.

#### 4.6 Benchmark 6

Lastly, we allow for B-mesons to decay into the neutralino via  $B^\pm \rightarrow \tilde{\chi}_1^0 + \tau^\pm$  and  $B^0 \rightarrow \tilde{\chi}_1^0 + \nu_\tau$  by setting  $\lambda'_{313} \neq 0$ . The only kinematically allowed decay mode is the radiative mode via the b-quark loop induced by  $\lambda'_{333}$ .

Isocurves for this benchmark (Fig. 8) depict a lot of characteristics we discussed in the previous benchmarks. Because of the large tau mass, we observe a small kink at the kinematic threshold for the charged decays. The greatest sensitivity reach is observed for ANUBIS with  $\lambda'/m^2 \approx 1.9 \times 10^{-9} \text{ GeV}^{-2}$ , while FASER is the least sensitive. As in benchmark 4, for  $m_{\tilde{\chi}_1^0} > 500 \text{ MeV}$  and benchmark 5, the initial mesons decay promptly, so that displaced decays do not affect the isocurves. Hence, our simulation agrees with the results for FASER and FASER2 of Ref. [70].



**Figure 7:** 3-event isocurves in the  $\lambda'/m_{\text{SUSY}}^2$  vs.  $m_{\tilde{\chi}_1^0}$  plane for benchmark 5. We assume mass degenerate sfermions. Previous results from Ref. [70] are presented as dotted lines. The gray shaded area represents already excluded coupling regions for  $\lambda'_{222}$  assuming  $m_{\text{SUSY}} = 1$  TeV.

## 5 Conclusions

We have analyzed the case of a light [ $m_{\tilde{\chi}_1^0} < \mathcal{O}(1.5 \text{ GeV})$ ] long-lived neutralino within supersymmetry with broken R-parity in the context of the LHC at CERN, with additional remote detectors: ANUBIS, CODEX-b, FACET, FASER, FASER2, MAPP, MAPP2, and MATHUSLA. Such a light neutralino is consistent with all current experimental constraints. We have simulated the production of the neutralinos via rare meson decays and defined six benchmark scenarios according to the dominant production channel: pions, kaons, a mixture of kaons and  $D$ -mesons, just  $D$ -mesons, or via  $B$ -mesons. In all cases, we have chosen the solely non-vanishing R-parity violating coupling such that the radiative neutralino decay  $\tilde{\chi}_1^0 \rightarrow \gamma + \nu$  is dominant. The corresponding benchmark characteristics are summarized in Table 4. The main purpose of this work is to analyze the sensitivity of the above detectors to this radiative mode. We have extended the previous work in Ref. [70], which primarily focused on FASER and FASER2, to analyze the other proposed detectors. In addition, we have improved the simulation by taking into account the finite decay length of the parent meson, which enhances the sensitivity as discussed in Sec. 4.1 and depicted in Figs. 2 and 3.

Our main results are presented in Fig. 1 for benchmark 1, Fig. 4, for benchmark

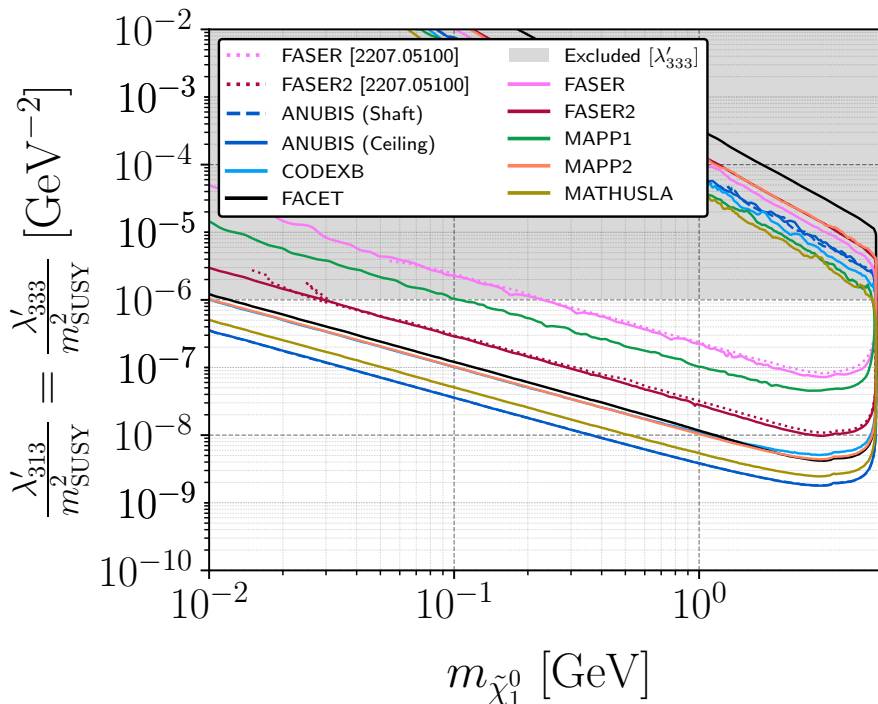


**Figure 8:** 3-event isocurves in the  $\lambda/m_{\text{SUSY}}^2$  vs.  $m_{\tilde{\chi}_1^0}$  plane for benchmark 6. We assume mass degenerate sfermions and equal coupling strengths for  $\lambda'_{313}$  and  $\lambda'_{333}$ . Previous results from Ref. [70] are presented as dotted lines. The gray shaded area represents already excluded coupling regions, where the constraint for  $\lambda'_{333}$  is the strongest constraint assuming  $m_{\text{SUSY}} = 1$  TeV.

2, Fig. 5 for benchmark 3, Fig. 6 for benchmark 4, Fig. 7 for benchmark 5, and Fig. 8 for benchmark 6. Overall, accounting for existing low-energy bounds on the R-parity violating couplings, we find for all benchmarks and for all detectors an unexplored sensitivity range, allowing for potential discoveries. Among the considered experiments, ANUBIS generally is the most sensitive and FASER the least sensitive experiment to the scenarios studied here, while of course FASER has already taken data.

## Acknowledgments

HKD would like to thank the Universiteit van Amsterdam and the Nikhef Theory Group for their hospitality while part of this work was completed. We thank Felix Kling, Florian Bernlochner, and Matthias Schott for discussions.

## References

- [1] J. Wess and B. Zumino, “Supergauge transformations in four dimensions,” *Nuclear Physics B* **70** no. 1, (1974) 39–50.
- [2] J. Wess and B. Zumino, “A lagrangian model invariant under supergauge transformations,” *Physics Letters B* **49** no. 1, (1974) 52–54.
- [3] R. Haag, J. T. Lopuszanski, and M. Sohnius, “All Possible Generators of Supersymmetries of the s Matrix,” *Nucl. Phys. B* **88** (1975) 257.
- [4] H. P. Nilles, “Supersymmetry, Supergravity and Particle Physics,” *Phys. Rept.* **110** (1984) 1–162.
- [5] H. E. Haber and G. L. Kane, “The Search for Supersymmetry: Probing Physics Beyond the Standard Model,” *Phys. Rept.* **117** (1985) 75–263.
- [6] S. P. Martin, “A Supersymmetry primer,” *Adv. Ser. Direct. High Energy Phys.* **18** (1998) 1–98, [arXiv:hep-ph/9709356](#).
- [7] H. Baer and X. Tata, *Weak scale supersymmetry: From superfields to scattering events*. Cambridge University Press, 5, 2006.
- [8] H. K. Dreiner, H. E. Haber, and S. P. Martin, *From Spinors to Supersymmetry*. Cambridge University Press, Cambridge, UK, 7, 2023.
- [9] M. J. G. Veltman, “The Infrared - Ultraviolet Connection,” *Acta Phys. Polon. B* **12** (1981) 437.
- [10] L. Lee, C. Ohm, A. Soffer, and T.-T. Yu, “Collider Searches for Long-Lived Particles Beyond the Standard Model,” *Prog. Part. Nucl. Phys.* **106** (2019) 210–255, [arXiv:1810.12602 \[hep-ph\]](#). [Erratum: *Prog.Part.Nucl.Phys.* 122, 103912 (2022)].
- [11] J. Alimena *et al.*, “Searching for long-lived particles beyond the Standard Model at the Large Hadron Collider,” *J. Phys. G* **47** no. 9, (2020) 090501, [arXiv:1903.04497 \[hep-ex\]](#).
- [12] C. Cesarotti, “Probing New Gauge Forces with a High-Energy Muon Beam-Dump Experiment,” *Physical Review Letters* **130** (2023) 071803.
- [13] K. Jodłowski and S. Trojanowski, “Neutrino beam-dump experiment with FASER at the LHC,” *JHEP* **05** (2021) 191, [arXiv:2011.04751 \[hep-ph\]](#).
- [14] **LZ** Collaboration, J. Aalbers *et al.*, “Search for new physics in low-energy electron recoils from the first LZ exposure,” *Phys. Rev. D* **108** no. 7, (2023) 072006, [arXiv:2307.15753 \[hep-ex\]](#).
- [15] **Planck** Collaboration, N. Aghanim *et al.*, “Planck 2018 results. VI. Cosmological parameters,” *Astron. Astrophys.* **641** (2020) A6, [arXiv:1807.06209 \[astro-ph.CO\]](#). [Erratum: *Astron.Astrophys.* 652, C4 (2021)].

- [16] **Super-Kamiokande** Collaboration, K. Abe *et al.*, “Atmospheric neutrino oscillation analysis with external constraints in Super-Kamiokande I-IV,” *Phys. Rev. D* **97** no. 7, (2018) 072001, [arXiv:1710.09126](#) [[hep-ex](#)].
- [17] **IceCube** Collaboration, M. G. Aartsen *et al.*, “Searches for Extended and Point-like Neutrino Sources with Four Years of IceCube Data,” *Astrophys. J.* **796** no. 2, (2014) 109, [arXiv:1406.6757](#) [[astro-ph.HE](#)].
- [18] **ATLAS** Collaboration, G. Aad *et al.*, “The ATLAS Experiment at the CERN Large Hadron Collider,” *JINST* **3** (2008) S08003.
- [19] **ATLAS** Collaboration, G. Aad *et al.*, “The ATLAS experiment at the CERN Large Hadron Collider: a description of the detector configuration for Run 3,” *JINST* **19** no. 05, (2024) P05063, [arXiv:2305.16623](#) [[physics.ins-det](#)].
- [20] **CMS Collaboration** Collaboration, S. Chatrchyan *et al.*, “The CMS Experiment at the CERN LHC,” *JINST* **3** (2008) S08004.
- [21] **CMS** Collaboration, A. Hayrapetyan *et al.*, “Development of the CMS detector for the CERN LHC Run 3,” *JINST* **19** no. 05, (2024) P05064, [arXiv:2309.05466](#) [[physics.ins-det](#)].
- [22] **ATLAS** Collaboration, G. Aad *et al.*, “Search for supersymmetry in final states with missing transverse momentum and three or more b-jets in 139 fb<sup>-1</sup> of proton–proton collisions at  $\sqrt{s} = 13$  TeV with the ATLAS detector,” *Eur. Phys. J. C* **83** no. 7, (2023) 561, [arXiv:2211.08028](#) [[hep-ex](#)].
- [23] **CMS** Collaboration, T. C. Collaboration *et al.*, “Search for supersymmetry in proton-proton collisions at 13 TeV in final states with jets and missing transverse momentum,” *JHEP* **10** (2019) 244, [arXiv:1908.04722](#) [[hep-ex](#)].
- [24] **Particle Data Group** Collaboration, S. Navas *et al.*, “Review of particle physics,” *Phys. Rev. D* **110** no. 3, (2024) 030001.
- [25] **ATLAS** Collaboration, G. Aad *et al.*, “A search for top-squark pair production, in final states containing a top quark, a charm quark and missing transverse momentum, using the 139 fb<sup>-1</sup> of pp collision data collected by the ATLAS detector,” *JHEP* **07** (2024) 250, [arXiv:2402.12137](#) [[hep-ex](#)].
- [26] **CMS** Collaboration, V. Chekhovsky *et al.*, “Search for top squarks in final states with many light-flavor jets and 0, 1, or 2 charged leptons in proton-proton collisions at  $\sqrt{s} = 13$  TeV,” *JHEP* **10** (2025) 236, [arXiv:2506.08825](#) [[hep-ex](#)].
- [27] L. E. Ibanez and G. G. Ross, “Discrete gauge symmetries and the origin of baryon and lepton number conservation in supersymmetric versions of the standard model,” *Nucl. Phys. B* **368** (1992) 3–37.
- [28] H. K. Dreiner, C. Luhn, and M. Thormeier, “What is the discrete gauge symmetry of the MSSM?,” *Phys. Rev. D* **73** (2006) 075007, [arXiv:hep-ph/0512163](#).
- [29] H. K. Dreiner, C. Luhn, H. Murayama, and M. Thormeier, “Baryon triality and

- neutrino masses from an anomalous flavor U(1),” *Nucl. Phys. B* **774** (2007) 127–167, [arXiv:hep-ph/0610026](#).
- [30] H. K. Dreiner, M. Hahn, and C. Luhn, “What is the discrete gauge symmetry of the R-parity violating MSSM?,” *Phys. Rev. D* **86** (2012) 055012, [arXiv:1206.6305 \[hep-ph\]](#).
- [31] P. Minkowski, “ $\mu \rightarrow e\gamma$  at a Rate of One Out of  $10^9$  Muon Decays?,” *Phys. Lett. B* **67** (1977) 421–428.
- [32] H. K. Dreiner, J. S. Kim, O. Lebedev, and M. Thormeier, “Supersymmetric Jarlskog invariants: The Neutrino sector,” *Phys. Rev. D* **76** (2007) 015006, [arXiv:hep-ph/0703074](#).
- [33] H. K. Dreiner, C. Luhn, H. Murayama, and M. Thormeier, “Proton Hexality from an Anomalous Flavor U(1) and Neutrino Masses: Linking to the String Scale,” *Nucl. Phys. B* **795** (2008) 172–200, [arXiv:0708.0989 \[hep-ph\]](#).
- [34] H. K. Dreiner and S. Grab, “All Possible Lightest Supersymmetric Particles in R-Parity Violating mSUGRA,” *Phys. Lett. B* **679** (2009) 45–50, [arXiv:0811.0200 \[hep-ph\]](#).
- [35] K. Desch, S. Fleischmann, P. Wienemann, H. K. Dreiner, and S. Grab, “Stau as the Lightest Supersymmetric Particle in R-Parity Violating SUSY Models: Discovery Potential with Early LHC Data,” *Phys. Rev. D* **83** (2011) 015013, [arXiv:1008.1580 \[hep-ph\]](#).
- [36] D. Dercks, H. Dreiner, M. E. Krauss, T. Opferkuch, and A. Reinert, “R-Parity Violation at the LHC,” *Eur. Phys. J. C* **77** no. 12, (2017) 856, [arXiv:1706.09418 \[hep-ph\]](#).
- [37] L. J. Hall and M. Suzuki, “Explicit R-Parity Breaking in Supersymmetric Models,” *Nucl. Phys. B* **231** (1984) 419–444.
- [38] H. K. Dreiner and G. G. Ross, “R-parity violation at hadron colliders,” *Nucl. Phys. B* **365** (1991) 597–613.
- [39] P. Bittar, S. Roy, and C. E. M. Wagner, “R-parity violation and 8 TeV four-jet events at the LHC: a falsification opportunity for Wagner’s Rule,” [arXiv:2509.09062 \[hep-ph\]](#).
- [40] H. K. Dreiner, Y. S. Koay, D. Köhler, V. M. Lozano, J. Montejó Berlingen, S. Nangia, and N. Strobbe, “The ABC of RPV: classification of R-parity violating signatures at the LHC for small couplings,” *JHEP* **07** (2023) 215, [arXiv:2306.07317 \[hep-ph\]](#).
- [41] H. K. Dreiner, M. Hank, Y. S. Koay, M. Schürmann, R. Sengupta, A. Shah, N. Strobbe, and E. Thomson, “The ABC of RPV. Part II. Classification of R-parity violating signatures from UDD couplings and their coverage at the LHC,” *JHEP* **06** (2025) 258, [arXiv:2503.03830 \[hep-ph\]](#).

- [42] B. C. Allanach, A. Dedes, and H. K. Dreiner, “R parity violating minimal supergravity model,” *Phys. Rev. D* **69** (2004) 115002, [arXiv:hep-ph/0309196](#). [Erratum: *Phys.Rev.D* 72, 079902 (2005)].
- [43] R. Hempfling, “Neutrino masses and mixing angles in SUSY GUT theories with explicit R-parity breaking,” *Nucl. Phys. B* **478** (1996) 3–30, [arXiv:hep-ph/9511288](#).
- [44] B. C. Allanach, A. Dedes, and H. K. Dreiner, “Two loop supersymmetric renormalization group equations including R-parity violation and aspects of unification,” *Phys. Rev. D* **60** (1999) 056002, [arXiv:hep-ph/9902251](#). [Erratum: *Phys.Rev.D* 86, 039906 (2012)].
- [45] D. Choudhury, H. K. Dreiner, P. Richardson, and S. Sarkar, “A Supersymmetric solution to the KARMEN time anomaly,” *Phys. Rev. D* **61** (2000) 095009, [arXiv:hep-ph/9911365](#).
- [46] A. Dedes, H. K. Dreiner, and P. Richardson, “Attempts at explaining the NuTeV observation of dimuon events,” *Phys. Rev. D* **65** (2001) 015001, [arXiv:hep-ph/0106199](#).
- [47] I. Gogoladze, J. D. Lykken, C. Macesanu, and S. Nandi, “Implications of a Massless Neutralino for Neutrino Physics,” *Phys. Rev. D* **68** (2003) 073004, [arXiv:hep-ph/0211391](#).
- [48] H. K. Dreiner, C. Hanhart, U. Langenfeld, and D. R. Phillips, “Supernovae and light neutralinos: SN1987A bounds on supersymmetry revisited,” *Phys. Rev. D* **68** (2003) 055004, [arXiv:hep-ph/0304289](#).
- [49] H. K. Dreiner, S. Heinemeyer, O. Kittel, U. Langenfeld, A. M. Weber, and G. Weiglein, “Mass Bounds on a Very Light Neutralino,” *Eur. Phys. J. C* **62** (2009) 547–572, [arXiv:0901.3485](#) [hep-ph].
- [50] H. K. Dreiner, M. Hanussek, J. S. Kim, and S. Sarkar, “Gravitino cosmology with a very light neutralino,” *Phys. Rev. D* **85** (2012) 065027, [arXiv:1111.5715](#) [hep-ph].
- [51] B. W. Lee and S. Weinberg, “Cosmological Lower Bound on Heavy Neutrino Masses,” *Phys. Rev. Lett.* **39** (1977) 165–168.
- [52] D. Hooper and T. Plehn, “Supersymmetric dark matter: How light can the LSP be?,” *Phys. Lett. B* **562** (2003) 18–27, [arXiv:hep-ph/0212226](#).
- [53] G. Belanger, F. Boudjema, A. Pukhov, and S. Rosier-Lees, “A Lower limit on the neutralino mass in the MSSM with nonuniversal gaugino masses,” in *10th International Conference on Supersymmetry and Unification of Fundamental Interactions (SUSY02)*, pp. 919–924. 12, 2002. [arXiv:hep-ph/0212227](#).
- [54] L. Calibbi, J. M. Lindert, T. Ota, and Y. Takahashi, “LHC Tests of Light Neutralino Dark Matter without Light Sfermions,” *JHEP* **11** (2014) 106, [arXiv:1410.5730](#) [hep-ph].

- [55] R. K. Barman, G. Bélanger, B. Bhattacharjee, R. M. Godbole, and R. Sengupta, “Is Light Neutralino Thermal Dark Matter in the Phenomenological Minimal Supersymmetric Standard Model Ruled Out?,” *Phys. Rev. Lett.* **131** no. 1, (2023) 011802, [arXiv:2207.06238 \[hep-ph\]](#).
- [56] R. K. Barman, G. Bélanger, B. Bhattacharjee, R. Godbole, and R. Sengupta, “Current status of the light neutralino thermal dark matter in the phenomenological MSSM,” *Phys. Rev. D* **111** no. 1, (2025) 015014, [arXiv:2402.07991 \[hep-ph\]](#).
- [57] H. K. Dreiner, “An Introduction to explicit R-parity violation,” *Adv. Ser. Direct. High Energy Phys.* **21** (2010) 565–583, [arXiv:hep-ph/9707435](#).
- [58] R. Barbier *et al.*, “R-parity violating supersymmetry,” *Phys. Rept.* **420** (2005) 1–202, [arXiv:hep-ph/0406039](#).
- [59] F. Domingo and H. K. Dreiner, “Decays of a bino-like particle in the low-mass regime,” *SciPost Phys.* **14** no. 5, (2023) 134, [arXiv:2205.08141 \[hep-ph\]](#).
- [60] S. Dawson, “R-Parity Breaking in Supersymmetric Theories,” *Nucl. Phys. B* **261** (1985) 297–318.
- [61] S. Ambrosanio, G. D. Kribs, and S. P. Martin, “Signals for gauge-mediated supersymmetry breaking models at the CERN LEP2 collider,” *Phys. Rev. D* **56** (1997) 1761–1777.
- [62] R. Essig *et al.*, “Working Group Report: New Light Weakly Coupled Particles,” in *Snowmass 2013: Snowmass on the Mississippi*. 10, 2013. [arXiv:1311.0029 \[hep-ph\]](#).
- [63] T. Appelquist, H.-C. Cheng, and B. A. Dobrescu, “Bounds on universal extra dimensions,” *Phys. Rev. D* **64** (2001) 035002, [arXiv:hep-ph/0012100](#).
- [64] **ATLAS** Collaboration, G. Aad *et al.*, “Search for new phenomena in events with a photon and missing transverse momentum in  $pp$  collisions at  $\sqrt{s} = 8$  TeV with the ATLAS detector,” *Phys. Rev. D* **91** no. 1, (2015) 012008, [arXiv:1411.1559 \[hep-ex\]](#). [Erratum: *Phys.Rev.D* 92, 059903 (2015)].
- [65] **ATLAS** Collaboration, M. Aaboud *et al.*, “Search for photonic signatures of gauge-mediated supersymmetry in 13 TeV  $pp$  collisions with the ATLAS detector,” *Phys. Rev. D* **97** no. 9, (2018) 092006, [arXiv:1802.03158 \[hep-ex\]](#).
- [66] **CMS** Collaboration, S. Chatrchyan *et al.*, “Search for Long-Lived Particles Decaying to Photons and Missing Energy in Proton-Proton Collisions at  $\sqrt{s} = 7$  TeV,” *Phys. Lett. B* **722** (2013) 273–294, [arXiv:1212.1838 \[hep-ex\]](#).
- [67] **CMS** Collaboration, A. M. Sirunyan *et al.*, “Search for gauge-mediated supersymmetry in events with at least one photon and missing transverse momentum in  $pp$  collisions at  $\sqrt{s} = 13$  TeV,” *Phys. Lett. B* **780** (2018) 118–143, [arXiv:1711.08008 \[hep-ex\]](#).

- [68] **CMS** Collaboration, A. M. Sirunyan *et al.*, “Search for supersymmetry in final states with photons and missing transverse momentum in proton-proton collisions at 13 TeV,” *JHEP* **06** (2019) 143, [arXiv:1903.07070 \[hep-ex\]](#).
- [69] **CMS** Collaboration, A. M. Sirunyan *et al.*, “Search for new physics in final states with a single photon and missing transverse momentum in proton-proton collisions at  $\sqrt{s} = 13$  TeV,” *JHEP* **02** (2019) 074, [arXiv:1810.00196 \[hep-ex\]](#).
- [70] H. K. Dreiner, D. Köhler, S. Nangia, and Z. S. Wang, “Searching for a single photon from lightest neutralino decays in R-parity-violating supersymmetry at FASER,” *JHEP* **02** (2023) 120, [arXiv:2207.05100 \[hep-ph\]](#).
- [71] **FASER** Collaboration, A. Ariga *et al.*, “Technical Proposal for FASER: ForwArd Search ExpeRiment at the LHC,” [arXiv:1812.09139 \[physics.ins-det\]](#).
- [72] O. Salin, “FASER2: Detector Design and Performance,” Tech. Rep. CERN-PBC-NOTE-2022-005, CERN, 2022. <https://cds.cern.ch/record/2927003>.
- [73] **FASER Collaboration** Collaboration, A. Ariga *et al.*, “Faser’s physics reach for long-lived particles,” *Phys. Rev. D* **99** (2019) 095011, [arXiv:1811.12522](#).
- [74] S. Cerci *et al.*, “FACET: A new long-lived particle detector in the very forward region of the CMS experiment,” *JHEP* **06** (2022) 110, [arXiv:2201.00019 \[hep-ex\]](#).
- [75] D. Curtin *et al.*, “Long-lived particles at the energy frontier: The mathusla physics case,” *Rept. Prog. Phys.* **82** (2019) 116201, [arXiv:1806.07396](#).
- [76] V. V. Gligorov, S. Knapen, M. Papucci, and D. J. Robinson, “Searching for Long-lived Particles: A Compact Detector for Exotics at LHCb,” *Phys. Rev. D* **97** no. 1, (2018) 015023, [arXiv:1708.09395 \[hep-ph\]](#).
- [77] **CODEX-b** Collaboration, G. Aielli *et al.*, “Technical design report for the CODEX- $\beta$  demonstrator,” *JINST* **20** no. 07, (2025) T07007, [arXiv:2406.12880 \[physics.ins-det\]](#).
- [78] M. Bauer, O. Brandt, L. Lee, and C. Ohm, “ANUBIS: Proposal to search for long-lived neutral particles in CERN service shafts,” [arXiv:1909.13022 \[physics.ins-det\]](#).
- [79] **MoEDAL-MAPP** Collaboration, B. Acharya *et al.*, “MoEDAL-MAPP, an LHC Dedicated Detector Search Facility,” in *Snowmass 2021*. 9, 2022. [arXiv:2209.03988 \[hep-ph\]](#).
- [80] **DUNE** Collaboration, B. Abi *et al.*, “Deep Underground Neutrino Experiment (DUNE), Far Detector Technical Design Report, Volume I Introduction to DUNE,” *JINST* **15** no. 08, (2020) T08008, [arXiv:2002.02967 \[physics.ins-det\]](#).
- [81] **DUNE** Collaboration, B. Abi *et al.*, “Deep Underground Neutrino Experiment (DUNE), Far Detector Technical Design Report, Volume II: DUNE Physics,” [arXiv:2002.03005 \[hep-ex\]](#).

- [82] **DUNE** Collaboration, B. Abi *et al.*, “The DUNE Far Detector Interim Design Report, Volume 3: Dual-Phase Module,” [arXiv:1807.10340](#) [[physics.ins-det](#)].
- [83] **DUNE** Collaboration, B. Abi *et al.*, “Deep Underground Neutrino Experiment (DUNE), Far Detector Technical Design Report, Volume IV: Far Detector Single-phase Technology,” *JINST* **15** no. 08, (2020) T08010, [arXiv:2002.03010](#) [[physics.ins-det](#)].
- [84] J. de Vries, H. K. Dreiner, and D. Schmeier, “R-Parity Violation and Light Neutralinos at SHiP and the LHC,” *Phys. Rev. D* **94** no. 3, (2016) 035006, [arXiv:1511.07436](#) [[hep-ph](#)].
- [85] **SHiP** Collaboration, C. Ahdida *et al.*, “Sensitivity of the SHiP experiment to Heavy Neutral Leptons,” *JHEP* **04** (2019) 077, [arXiv:1811.00930](#) [[hep-ph](#)].
- [86] **SHiP** Collaboration, C. Ahdida *et al.*, “The SHiP experiment at the proposed CERN SPS Beam Dump Facility,” *Eur. Phys. J. C* **82** no. 5, (2022) 486, [arXiv:2112.01487](#) [[physics.ins-det](#)].
- [87] **JUNO** Collaboration, A. Abusleme *et al.*, “JUNO physics and detector,” *Prog. Part. Nucl. Phys.* **123** (2022) 103927, [arXiv:2104.02565](#) [[hep-ex](#)].
- [88] M. Hirsch, M. A. Diaz, W. Porod, J. C. Romao, and J. W. F. Valle, “Neutrino masses and mixings from supersymmetry with bilinear R parity violation: A Theory for solar and atmospheric neutrino oscillations,” *Phys. Rev. D* **62** (2000) 113008, [arXiv:hep-ph/0004115](#). [Erratum: *Phys.Rev.D* 65, 119901 (2002)].
- [89] F. de Campos, O. J. P. Eboli, M. B. Magro, W. Porod, D. Restrepo, M. Hirsch, and J. W. F. Valle, “Probing bilinear R-parity violating supergravity at the LHC,” *JHEP* **05** (2008) 048, [arXiv:0712.2156](#) [[hep-ph](#)].
- [90] L. J. Hall and M. Suzuki, “Explicit R-Parity Breaking in Supersymmetric Models,” *Nuclear Physics B* **231** (1984) 419–444.
- [91] H. K. Dreiner and M. Thormeier, “Supersymmetric Froggatt-Nielsen Models with Baryon and Lepton Number Violation,” *Physical Review D* **69** (2004) 053002, [hep-ph/0305270](#).
- [92] M. Chemtob, “Phenomenological constraints on broken R parity symmetry in supersymmetry models,” *Prog. Part. Nucl. Phys.* **54** (2005) 71–191, [arXiv:hep-ph/0406029](#).
- [93] N. Chamoun, F. Domingo, and H. K. Dreiner, “Nucleon Decay in the R-Parity Violating MSSM,” *Physical Review D* **104** no. 1, (2021) 015020, [arXiv:2012.11623](#) [[hep-ph](#)].
- [94] **Particle Data Group** Collaboration, S. Navas *et al.*, “Review of Particle Physics,” *Physical Review D* **110** no. 3, (2024) 030001.
- [95] F. Domingo, H. K. Dreiner, D. Köhler, S. Nangia, and A. Shah, “A novel proton decay signature at DUNE, JUNO, and Hyper-K,” *JHEP* **05** (2024) 258, [arXiv:2403.18502](#) [[hep-ph](#)].

- [96] H. K. Dreiner, J. Y. Günther, and Z. S. Wang, “ $R$ -parity violation and light neutralinos at ANUBIS and MAPP,” *Phys. Rev. D* **103** no. 7, (2021) 075013, [arXiv:2008.07539 \[hep-ph\]](#).
- [97] Z. S. Wang, H. K. Dreiner, and J. Y. Günther, “The decay  $B \rightarrow K + \nu + \bar{\nu}$  at Belle II and a massless bino in  $R$ -parity-violating supersymmetry,” *Eur. Phys. J. C* **85** no. 1, (2025) 66, [arXiv:2309.03727 \[hep-ph\]](#).
- [98] H. K. Dreiner, M. Hanussek, and S. Grab, “Bounds on  $R$ -parity Violating Couplings at the Grand Unification Scale from Neutrino Masses,” *Phys. Rev. D* **82** (2010) 055027, [arXiv:1005.3309 \[hep-ph\]](#).
- [99] H. K. Dreiner and S. Grab, “All Possible Lightest Supersymmetric Particles in  $R$ -Parity Violating mSUGRA Models and their Signals at the LHC,” *AIP Conf. Proc.* **1200** no. 1, (2010) 358–361, [arXiv:0909.5407 \[hep-ph\]](#).
- [100] D. Dercks, J. De Vries, H. K. Dreiner, and Z. S. Wang, “ $R$ -parity Violation and Light Neutralinos at CODEX-b, FASER, and MATHUSLA,” *Phys. Rev. D* **99** no. 5, (2019) 055039, [arXiv:1810.03617 \[hep-ph\]](#).
- [101] J. Y. Günther, J. de Vries, H. K. Dreiner, Z. S. Wang, and G. Zhou, “Long-lived neutral fermions at the DUNE near detector,” *JHEP* **01** (2024) 108, [arXiv:2310.12392 \[hep-ph\]](#).
- [102] B. C. Allanach, A. Dedes, and H. K. Dreiner, “Bounds on  $R$ -parity violating couplings at the weak scale and at the GUT scale,” *Phys. Rev. D* **60** (1999) 075014, [arXiv:hep-ph/9906209](#).
- [103] J. De Vries, H. K. Dreiner, J. Y. Günther, Z. S. Wang, and G. Zhou, “Long-lived Sterile Neutrinos at the LHC in Effective Field Theory,” *JHEP* **03** (2021) 148, [arXiv:2010.07305 \[hep-ph\]](#).
- [104] F. Kling and S. Trojanowski, “Forward experiment sensitivity estimator for the LHC and future hadron colliders,” *Phys. Rev. D* **104** no. 3, (2021) 035012, [arXiv:2105.07077 \[hep-ph\]](#).
- [105] C. Bierlich *et al.*, “A comprehensive guide to the physics and usage of PYTHIA 8.3,” *SciPost Phys. Codeb.* **2022** (2022) 8, [arXiv:2203.11601 \[hep-ph\]](#).
- [106] M. Fieg, F. Kling, H. Schulz, and T. Sjöstrand, “Tuning pythia for forward physics experiments,” *Phys. Rev. D* **109** no. 1, (2024) 016010, [arXiv:2309.08604 \[hep-ph\]](#).
- [107] J. L. Feng, I. Galon, F. Kling, and S. Trojanowski, “ForwArd Search ExpeRiment at the LHC,” *Phys. Rev. D* **97** no. 3, (2018) 035001, [arXiv:1708.09389 \[hep-ph\]](#).
- [108] **FASER** Collaboration, A. Ariga *et al.*, “FASER’s physics reach for long-lived particles,” *Phys. Rev. D* **99** no. 9, (2019) 095011, [arXiv:1811.12522 \[hep-ph\]](#).
- [109] **ANUBIS** Collaboration, A. Shah, “Searches for long-lived particles with the ANUBIS experiment,” *PoS EPS-HEP2023* (2024) 051, [arXiv:2401.11604 \[hep-ex\]](#).

- [110] **CODEX-b** Collaboration, G. Aielli *et al.*, “Expression of interest for the CODEX-b detector,” *Eur. Phys. J. C* **80** no. 12, (2020) 1177, [arXiv:1911.00481 \[hep-ex\]](#).
- [111] **CODEX-b** Collaboration, E. X. Rodriguez Fernandez, “COmpact DETector for EXotics at LHCb: CODEX-b,” *PoS ICHEP2024* (2025) 1077.
- [112] J. L. Pinfold, “The MoEDAL experiment: a new light on the high-energy frontier,” *Phil. Trans. Roy. Soc. Lond. A* **377** no. 2161, (2019) 20190382.
- [113] **MoEDAL-MAPP** Collaboration, M. Kalliokoski, “The MAPP-1 Detector at LHC’s Run-3,” *PoS TIPP2023* (2025) 101.
- [114] J. P. Chou, D. Curtin, and H. J. Lubatti, “New Detectors to Explore the Lifetime Frontier,” *Phys. Lett. B* **767** (2017) 29–36, [arXiv:1606.06298 \[hep-ph\]](#).
- [115] D. Curtin *et al.*, “Long-Lived Particles at the Energy Frontier: The MATHUSLA Physics Case,” *Rept. Prog. Phys.* **82** no. 11, (2019) 116201, [arXiv:1806.07396 \[hep-ph\]](#).
- [116] **MATHUSLA** Collaboration, C. Alpigiani *et al.*, “An Update to the Letter of Intent for MATHUSLA: Search for Long-Lived Particles at the HL-LHC,” [arXiv:2009.01693 \[physics.ins-det\]](#).
- [117] **MATHUSLA** Collaboration, B. Aitken *et al.*, “MATHUSLA: An External Long-Lived Particle Detector to Maximize the Discovery Potential of the HL-LHC,” [arXiv:2504.01999 \[physics.ins-det\]](#).
- [118] M. Hirsch, H. V. Klapdor-Kleingrothaus, and S. G. Kovalenko, “New constraints on R-parity broken supersymmetry from neutrinoless double beta decay,” *Phys. Rev. Lett.* **75** (1995) 17–20.
- [119] P. D. Bolton, F. F. Deppisch, and P. S. B. Dev, “Neutrinoless double beta decay via light neutralinos in R-parity violating supersymmetry,” *JHEP* **03** (2022) 152, [arXiv:2112.12658 \[hep-ph\]](#).
- [120] R. Beltrán, G. Cottin, M. Hirsch, A. Titov, and Z. S. Wang, “Reinterpretation of searches for long-lived particles from meson decays,” *JHEP* **05** (2023) 031, [arXiv:2302.03216 \[hep-ph\]](#).